



Article

Environmental and Vegetative Controls on Soil CO₂ Efflux in Three Semiarid Ecosystems

Matthew C. Roby^{1,2}, Russell L. Scott^{2,*} , Greg A. Barron-Gafford^{3,4}, Erik P. Hamerlynck⁵ and David J. P. Moore¹

¹ School of Natural Resources and the Environment, University of Arizona, Tucson, AZ 85721, USA; mattroby@email.arizona.edu (M.C.R.); davidjpmoore@email.arizona.edu (D.J.P.M.)

² Southwest Watershed Research Center, USDA-ARS, Tucson, AZ 85719, USA

³ School of Geography & Development, University of Arizona, Tucson, AZ 85721, USA; gregbg@email.arizona.edu

⁴ College of Science, Biosphere 2, University of Arizona, Tucson, AZ 85721, USA

⁵ Eastern Oregon Agricultural Research Center, USDA-ARS, Burns, OR 97720, USA; erik.hamerlynck@ars.usda.gov

* Correspondence: russ.scott@ars.usda.gov; Tel.: +1-520-647-2971

Received: 27 October 2018; Accepted: 2 January 2019; Published: 8 January 2019



Abstract: Soil CO₂ efflux (F_{soil}) is a major component of the ecosystem carbon balance. Globally expansive semiarid ecosystems have been shown to influence the trend and interannual variability of the terrestrial carbon sink. Modeling F_{soil} in water-limited ecosystems remains relatively difficult due to high spatial and temporal variability associated with dynamics in moisture availability and biological activity. Measurements of the processes underlying variability in F_{soil} can help evaluate F_{soil} models for water-limited ecosystems. Here we combine automated soil chamber and flux tower data with models to investigate how soil temperature (T_s), soil moisture (θ), and gross ecosystem photosynthesis (GEP) control F_{soil} in semiarid ecosystems with similar climates and different vegetation types. Across grassland, shrubland, and savanna sites, θ regulated the relationship between F_{soil} and T_s , and GEP influenced F_{soil} magnitude. Thus, the combination of T_s , θ , and GEP controlled rates and patterns of F_{soil} . In a root exclusion experiment at the grassland, we found that growing season autotrophic respiration accounted for 45% of F_{soil} . Our modeling results indicate that a combination of T_s , θ , and GEP terms is required to model spatial and temporal dynamics in F_{soil} , particularly in deeper-rooted shrublands and savannas where coupling between GEP and shallow θ is weaker than in grasslands. Together, these results highlight that including θ and GEP in F_{soil} models can help reduce uncertainty in semiarid ecosystem carbon dynamics.

Keywords: soil respiration; drylands; water availability; spatial variation; temporal dynamics; pulses; photosynthesis; ecosystem respiration

1. Introduction

Semiarid ecosystems have been shown to impact global carbon dynamics [1,2]. Ecosystem respiration strongly influences net carbon balance [3] and contributes significantly to variability in the net carbon exchange of semiarid ecosystems [4,5]. Soil carbon dioxide (CO₂) efflux (F_{soil}) represents CO₂ efflux due to belowground plant and microbial respiration and biogeochemical processes, and is a major component of total ecosystem respiration [6,7]. Increased understanding of the processes underlying F_{soil} variation in globally expansive semiarid ecosystems is necessary to reduce uncertainty in terrestrial carbon dynamics.

While controls on respiration processes in more mesic regions are well documented [8,9], F_{soil} in water-limited ecosystems exhibits spatial and temporal variability associated with dynamics in

moisture availability and biological activity [10–16]. Compared to mesic sites, F_{soil} estimates in water-limited ecosystems are more uncertain, partially due to relatively sparse data in drylands despite the recent increase in measurements of F_{soil} globally [17]. Limitations in available data inhibit the development and evaluation of new F_{soil} models for application in water-limited ecosystems. Measurements that examine the processes underlying variability in F_{soil} across a variety of environmental and biological conditions would be useful to develop and evaluate models that recognize the role of temperature, moisture, and substrate limitation on carbon exchange [16,18], particularly in globally extensive drylands projected to expand in response to global change [19,20].

Multivariate models can be useful to represent how dynamics in substrate availability and environmental factors contribute to pulses and seasonality in the metabolic activity of water-limited ecosystems [21–24]. However, existing biogeochemical models largely represent respiration processes with static temperature sensitivity equations and empirical moisture functions predominantly developed in mesic regions [8,14,25,26]. In water limited-ecosystems, dynamics in soil moisture and photosynthesis strongly regulate F_{soil} over sub-seasonal to interannual timescales [9,27]. Soil moisture availability can influence the magnitude, temperature response, and seasonality of F_{soil} and can cause hysteresis between F_{soil} and its drivers [11,15,16,18,24,28–31]. Vegetation structure and function characteristics—including root distribution, hydraulic redistribution, root respiration, photosynthate exudation, and effects on microclimate—can influence the factors that control spatial and temporal variability in F_{soil} [16,22,32–35].

Previous studies in water-limited ecosystems have illustrated how F_{soil} varies with interacting environmental and vegetative factors. Variation in plant and soil characteristics modify the response of F_{soil} to changes in water availability and temperature [13,36], and vegetation structure impacts the timescales over which environmental and vegetative factors influence F_{soil} in mixed-vegetation ecosystems [34,37]. Despite advances in our understanding of dryland F_{soil} , representing how these interacting factors impact F_{soil} in heterogeneous ecosystems remains a modeling challenge.

Models are beginning to capture the effects of moisture availability and vegetation activity on the temperature dependency of F_{soil} [31]. Such model structures impose moisture constraints on F_{soil} [38] and assume that respiration processes are stimulated by canopy photosynthesis [39]. However, it is not well known if these new models can capture dynamics in F_{soil} associated with interacting environmental and vegetative factors across structurally diverse semiarid ecosystems.

Multisite measurements targeted to investigate the complex interactions between these drivers can help us determine if new F_{soil} models are broadly applicable in semiarid ecosystems. Trenched-plot experiments can help isolate the interacting effects of environmental and vegetative factors on F_{soil} [6,40–42]. Even if trenched-plots are unavailable, measurements from plots that differ in their distance from patchy vegetation can be used to assess how plants may be influencing F_{soil} through effects on microclimate and root activity [13,34,37].

In this study, we integrated data and modeling to investigate how environmental and vegetative factors influence F_{soil} across three semiarid sites. These sites were similar in climate forcing but differed in stand structure, with major differences in the amounts of grass, shrubs, and trees. The objectives of this study were to (1) combine automated soil chamber and flux tower data to investigate how soil temperature (T_s), soil moisture (θ), and gross ecosystem photosynthesis (GEP) regulate F_{soil} in semiarid grassland, shrubland, and savanna ecosystems; and (2) assess the ability of data-informed models to predict temporal variability in F_{soil} across three structurally diverse semiarid ecosystems. To achieve these objectives, we combined data from a grassland trenched-plot experiment with measurements from intercanopy and under-canopy plots in shrubland and savanna sites that differed in their proximity to vegetation. We then tested model performance at each site to determine if the mechanisms underlying variation in F_{soil} were broadly consistent across these ecosystems. We hypothesize that the combination of T_s , θ , and GEP control F_{soil} at each site, and that the relative explanatory value of model drivers varies among sites due to differences in how vegetation structure impacts coupling between shallow soil moisture and carbon exchange. Based on this hypothesis, we predict that the

relative explanatory value of θ and GEP will differ the most at sites with deeper rooting depths (savanna > shrubland > grassland) where GEP is less coupled to shallow soil moisture.

2. Materials and Methods

2.1. Site Description

This study was conducted at three AmeriFlux sites in southeast Arizona, USA. Kendall Grassland (grassland; AmeriFlux site ID: US-Wkg) is a warm-season, semiarid grassland dominated by perennial bunchgrasses (mainly, *Eragrostis lehmannia*). Lucky Hills Shrubland (shrubland; site ID: US-Whs) is a shrubland composed of a variety of Chihuahuan desert shrubs (*Larrea tridentata*, *Parthenium incanum*, *Acacia constricta*). Both sites are located within the USDA Agricultural Research Service Walnut Gulch Experimental Watershed. Santa Rita Mesquite Savanna (savanna; site ID: US-SRM) is a semiarid grassland that has experienced encroachment by velvet mesquite trees (*Prosopis velutina*). The savanna site is located in the Santa Rita Experimental Range, roughly 80 km west of the other sites. A detailed description of the sites can be found in a previous study [43]. The sites experience similar mean annual temperature (~ 17 °C) and mean annual precipitation (320–384 mm) but differ in their vegetative structure and productivity (Table 1 and Figure 1). Grass covers 37% of the grassland, whereas woody cover dominates the shrubland (40%) and savanna (35%). Canopy height and mean annual leaf area index increase from lowest to highest for the shrubland, grassland, and savanna. Roughly 60% of annual precipitation occurs in July–September, associated with the North American Monsoon.

Table 1. Description of the study sites.

	Walnut Gulch Kendall Grassland (Grassland)	Lucky Hills Shrubland (Shrubland)	Santa Rita Mesquite Savanna (Savanna)
Year	2017	2012	2015
Latitude, longitude (°)	31.7378° N, 109.9428° W	31.749° N, 110.052° W	31.822° N, 110.867° W
Elevation (m)	1530	1370	1120
Mean air temp. (°C)	15.6	17.6	19.0
Mean annual precip. (1971–2010; mm)	346	320	384
Mean annual GEP (g C m ⁻² year ⁻¹)	227	159	331
Mean LAI (MODIS)	0.30	0.25	0.37
Woody cover (%)	3	40	35
Perennial grass/forb cover (%)	37	3	15
Soil type	Very gravelly, sandy to fine sandy, and clayey loams	Gravelly sandy loams	Deep loamy sands
Plots	Grass (n = 4) Trenched (n = 4)	Shrub (n = 4) Intercanopy (n = 4)	Under tree (n = 2) Intercanopy (n = 3)

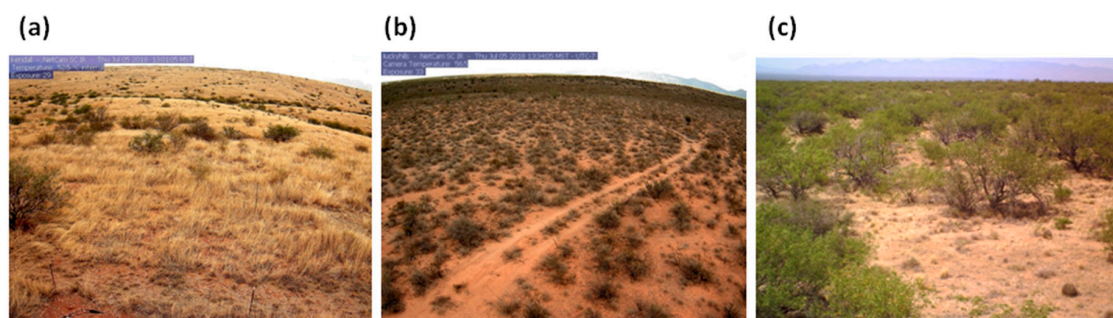


Figure 1. Webcam images depicting the vegetation type of the grassland (a), shrubland (b), and mesquite savanna (c) sites.

2.2. Soil CO₂ Efflux and Environmental Measurements

The net efflux of carbon dioxide (CO₂) at the soil-atmosphere interface (F_{soil}) was measured using an infrared gas analyzer coupled with automated soil chambers (LI-8100, LI-COR, Lincoln, NE, USA). Automated chambers were deployed at each site in plots near vegetation. Soil collars were inserted to a depth of 8–9 cm, leaving 2–3 cm of the collars exposed. We used the FV8100 Data File Viewer (LI-COR) to estimate F_{soil} by fitting an exponential regression to the rate of increase in CO₂ molar fraction over each 120 s measurement interval. We excluded F_{soil} estimates from fits with $R^2 < 0.90$ and values of $F_{soil} < -1$ or $>15 \mu\text{mol CO}_2 \text{ m}^{-2} \text{ s}^{-1}$.

In 2017, F_{soil} was measured twice per hour at the grassland using four chambers adjacent to patches of perennial bunchgrass (*Eragrostis lehmanniana*, “grass”). To exclude the effects of vegetation activity on F_{soil} , we added four additional chambers in bare plots and trenched each plot’s perimeter on 22 June 2017 prior to the summer rainy season, hereafter referred to as “trenched”. Trenches were dug to ~30 cm depth and lined with ground cover fabric to prevent root growth back into the plot. Roughly ~84% of the grass roots at this site are within the top 30 cm of soil [44]. We regularly weeded the trenched plots to ensure the soil was bare throughout the growing season. We assume CO₂ efflux measured in trenched plots represents heterotrophic respiration (R_h), while total F_{soil} measured in grass plots includes R_h and belowground autotrophic respiration (R_a). We define R_a as the difference between grass F_{soil} and trenched R_h . Supplementary measurements of T_s and θ were measured at a depth of 5 cm with a LI-COR temperature probe and a soil moisture probe (EC-5, Decagon, now METER Group, Washington, DC, USA), respectively. Beginning in June 2017, ECH₂O 5TM probes (METER Group) were used to measure 5 cm T_s and θ for all chambers at the site.

To extend our investigation across sites with differing vegetation structure, we also measured F_{soil} , T_s , and θ in the shrubland and savanna. In the shrubland in 2012, F_{soil} was measured every two hours using four chambers under creosote bush shrubs (*Larrea tridentata*) and four chambers located between the sparsely separated shrubs (~2 m from canopy drip lines). In the savanna in 2015, hourly F_{soil} was measured using three chambers installed halfway between the tree bole and drip line of velvet mesquite trees (*Prosopis velutina*) and from three chambers ~5 m from trees in the intercanopy space. A malfunctioning chamber at the savanna site was excluded from analysis, which reduced the number of tree plots to two. We measured 5 cm T_s and θ at the shrubland and savanna using LI-COR temperature probes and ECH₂O probes, respectively. Importantly, the intercanopy plots at the shrubland and savanna sites were not trenched and therefore were likely influenced by root activity.

2.3. Ecosystem Photosynthesis

To quantify how vegetation activity influences F_{soil} , ecosystem-scale carbon fluxes were measured using the eddy covariance technique. Details of the instrumentation and methods used at each site have been described previously [45]. Briefly, 30 min average net ecosystem exchange of CO₂ (NEE) was partitioned into gross ecosystem photosynthesis (GEP ; hereafter referred to as photosynthesis) and ecosystem respiration (R_{eco} ; [43]). An exponential function was fit to friction velocity-filtered nighttime NEE and air temperature over a ~5 day moving window to determine R_{eco} [46]. GEP was calculated as the difference between R_{eco} and NEE , with the sign convention of positive values for GEP and R_{eco} . A previous comparison of R_{eco} and F_{soil} at the savanna site [47] showed that integrated F_{soil} was greater than R_{eco} over the course of a growing season. This indicates that F_{soil} is systematically overestimated, or R_{eco} is underestimated, as R_{eco} should also account for aboveground respiration. If R_{eco} is underestimated, this would result in an underestimate of GEP . However, this systematic bias should not have a large impact on our modeling results so long as GEP and F_{soil} capture the temporal variability in these processes. This is because the empirical model coefficients described below are optimized to fit the data.

2.4. Data Analysis

At each site, plot means were calculated as the average of replicates. Missing data and outliers were replaced with the mean of replicates. Hourly means were used to examine the impact of θ on the relationship between F_{soil} and T_s . To investigate how water availability influenced the temperature response of F_{soil} at the grassland, we fit Equation (1) to data binned by θ quantiles in 10% increments.

Daily means were calculated from sub-daily measurements to account for differences in sampling rates among sites. The response of F_{soil} to recent carbon inputs was determined by regressing daily mean F_{soil} against daily mean GEP , and we used the Student's t -test to evaluate differences in regression parameters [48]. Daily means were used to investigate seasonality in carbon fluxes and environmental variables and to examine relationships between F_{soil} and GEP . We used the paired t -test to test for differences in daily mean F_{soil} and drivers between plots that varied in their distance from vegetation. At the grassland, we tested for differences between plots in the basal rate and temperature sensitivity of F_{soil} by testing for overlap in the 95% confidence intervals of coefficients determined by fitting Equation (1) described below.

2.5. Model Development

We used a modeling framework to investigate how the inclusion of environmental and vegetative terms influenced predicted spatial and temporal variation in F_{soil} . All models were based on an exponential temperature function [8]:

$$F_{soil} = F_{ref} e^{bT_s}, \quad (1)$$

where F_{soil} is soil CO_2 efflux ($\mu\text{mol } CO_2 \text{ m}^{-2} \text{ s}^{-1}$), F_{ref} is the basal F_{soil} when T_s is $0 \text{ } ^\circ\text{C}$ ($\mu\text{mol } CO_2 \text{ m}^{-2} \text{ s}^{-1}$), and b is the temperature sensitivity of F_{soil} . We supplemented temperature-based models with θ and GEP terms to represent the effects of moisture availability and vegetation activity on F_{soil} [31]. Moisture effects were incorporated into Equation (1) using a quadratic structure that reflects how excessively high or low θ suppresses F_{soil} [38,49,50] as:

$$F_{soil} = F_{ref,\theta} [1 - c(\theta - \theta_{opt})]^2 e^{bT_s}, \quad (2)$$

where θ_{opt} is the optimum θ value for which F_{soil} is greatest and c represents the sensitivity of F_{soil} to θ by controlling the slope of the exponential curve (higher values of c indicate stronger effects of θ). At each site we determined θ_{opt} by examining the response of daily mean F_{soil} to θ and visually estimating the value of θ associated with maximum F_{soil} . Following reference [31], we added a photosynthesis term to Equation (1) to represent the effects of T_s and GEP on F_{soil} using:

$$F_{soil} = F_{ref,GEP} \frac{\frac{GEP}{GEP_{max}} + n}{1 + n} e^{bT_s}, \quad (3)$$

where n represents the degree to which GEP drives F_{soil} relative to heterotrophic processes ($n = 0$ indicates strong GEP effect on F_{soil}) and GEP_{max} is the maximum value of GEP . The combined effects of temperature, moisture, and photosynthesis were represented by

$$F_{soil} = F_{ref,\theta,GEP} \frac{\frac{GEP}{GEP_{max}} + n}{1 + n} [1 - c(\theta - \theta_{opt})]^2 e^{bT_s}, \quad (4)$$

Models were fit using nonlinear least squares regression in which the coefficients were estimated using an iterative method based on starting values in Matlab (Mathworks, Inc., Natick, MA, USA). To account for differences in model complexity, model performance was assessed using the coefficient of determination (R^2), Akaike Information Criterion (AIC ; [51]), and root mean squared error ($RMSE$). We used cross-correlation to test for lags between daily mean F_{soil} and daily mean GEP . For sites with significant lag, we re-fit Equations (3) and (4) with optimum lag and assessed changes in model performance.

3. Results

3.1. Seasonality of Soil CO₂ Efflux

Across all sites, daily mean F_{soil} and GEP followed seasonal dynamics of changes in water availability (Figure 2a,c,d; Figures S1 and S2). At the grassland site with grass and trenched plots, a brief and limited spring growing season (DOY 75–100) was followed by low F_{soil} , GEP , and θ , despite increasing T_s (Figure 2a–d). Average pre-summer monsoon (DOY 0–175) daily mean F_{soil} for the grass plot was $0.52 \mu\text{mol CO}_2 \text{ m}^{-2} \text{ s}^{-1}$. During the monsoon (DOY 175–250), θ was high and average daily mean F_{soil} for the grass plot increased significantly to an average $2.3 \mu\text{mol CO}_2 \text{ m}^{-2} \text{ s}^{-1}$ ($p < 0.01$). Rates of GEP responded gradually to the onset of monsoon precipitation, whereas F_{soil} increased rapidly with θ . (Figure 2a,c,d). Post-monsoon (DOY 250–365) rates of F_{soil} and GEP decreased following seasonal decreases in GEP , θ and T_s (Figure 2a–d).

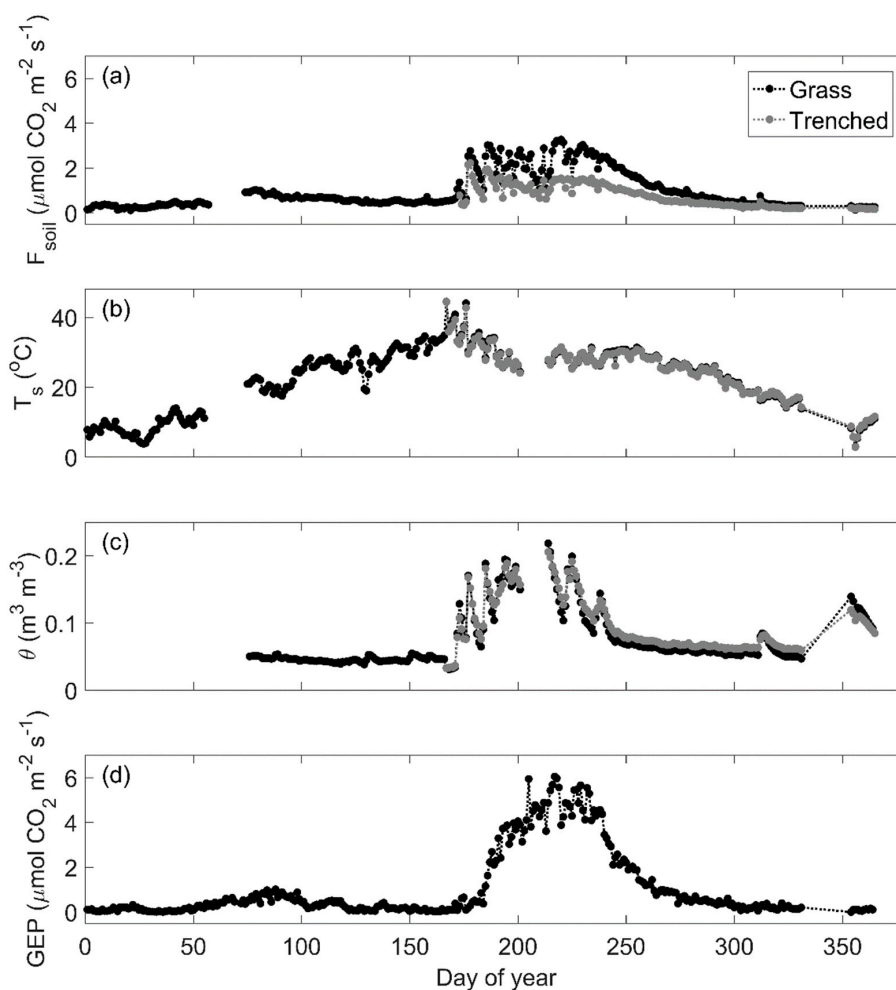


Figure 2. Seasonal pattern in 2017 of observed (a) daily mean soil CO₂ efflux (F_{soil}), (b) soil temperature (T_s), and (c) volumetric soil moisture (θ) for soil near patches of grass (black) and in bare, trenched intercanopy space (gray) from the grassland. Also shown is (d) daily mean gross ecosystem photosynthesis (GEP).

3.2. Environmental Controls on Soil CO₂ Efflux

Median F_{soil} increased with θ (Figures S3–S5), and daily mean θ contributed to 51–77% of the variation in daily mean F_{soil} at all sites. (Figures S6–S8). T_s explained significant variation in F_{soil} for high θ , but T_s and F_{soil} were weakly coupled when θ was low (Figure 3a). Since the amount of variation in F_{soil} explained by Equation (1) varied significantly with θ , we used the quantile fit

results (Figure 3a) and re-fit Equation (1) into wet (grass: $\theta > 7$ th quantile; trenched: $\theta > 6$ th quantile) and dry (grass: $\theta < 8$ th quantile; trenched: $\theta < 7$ th quantile) conditions. Rates of F_{soil} were generally low for dry conditions, despite increasing T_s , whereas F_{soil} increased strongly with T_s when the soil was wet (Figure 3b,c). Basal soil CO₂ efflux (F_{ref}) and the temperature sensitivity of F_{soil} (b) varied significantly with θ and differed between the grass and trenched plots (Figure 3b,c; $p < 0.01$). F_{ref} was 54% and 64% greater for wet than dry conditions at the grass and trenched plots, respectively. Between plots, grass F_{ref} was 63% and 73% greater than trenched F_{ref} for wet and dry conditions, respectively. Wet conditions were associated with greater b than dry conditions, and this difference was more pronounced in vegetated plots than in trenched ones. Similar to the grassland, wet conditions at the savanna corresponded with high F_{ref} and b ; however, the temperature response of F_{soil} at the savanna was more variable than at the grassland (Figure S9). Unexpectedly, F_{soil} did not show a clear response to T_s at the shrubland (Figure S10). For all sites, we found that T_s alone was not the only driver of F_{soil} and that even when accounting for variation in θ , significant variation in F_{soil} remained unexplained (Figure 3, Figures S9 and S10).

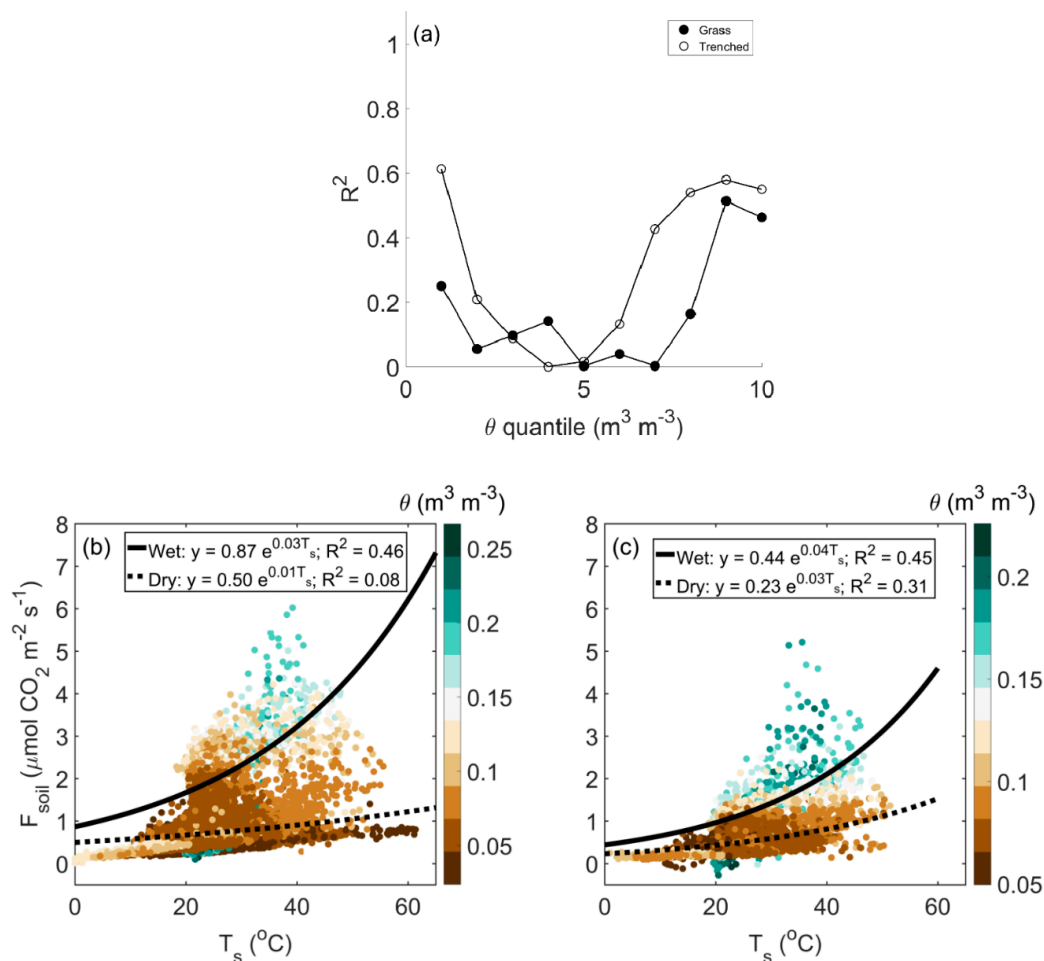


Figure 3. (a) Coefficient of determination (R^2) values from an exponential fit of soil CO₂ efflux (F_{soil}) to soil temperature (T_s), Equation (1), for different 10% quantiles of volumetric soil moisture (θ) at the grassland site. The influence of θ (color) on the temperature response of F_{soil} for grass (b) and trenched plots (c) with curves fit for wet and dry θ conditions.

3.3. Physiological Controls on Soil CO₂ Efflux

Although the seasonal pattern of F_{soil} at the grassland was similar for the grass and trenched plots, there were significant differences in the magnitude of daily mean F_{soil} between plots (Figure 2a)

that strongly correlated with daily mean GEP ($R^2 = 0.66$). Daily mean F_{soil} during the monsoon was significantly greater for the grass ($2.3 \mu\text{mol CO}_2 \text{ m}^{-2} \text{ s}^{-1}$) than trenched plots ($1.2 \mu\text{mol CO}_2 \text{ m}^{-2} \text{ s}^{-1}$; $p < 0.01$), despite similar T_s and θ ($p > 0.1$). Using the difference in F_{soil} between grass and trenched plots in the grassland, we estimate that belowground autotrophic (R_a) and heterotrophic (R_h) respiration accounted for 44% and 56% of cumulative growing season F_{soil} , respectively (Figure 4).

To investigate how plant activity influenced F_{soil} across sites with varying vegetation type and productivity, we examined the relationship between F_{soil} and GEP . Daily mean F_{soil} increased with daily mean GEP at all sites, and the rate of increase was greater for plots near vegetation (Figure 5; $p < 0.01$). At all sites, F_{soil} was 35–59% greater for plots near vegetation compared to plots that were either trenched (grassland only) or located further from vegetation (~2–5 m).

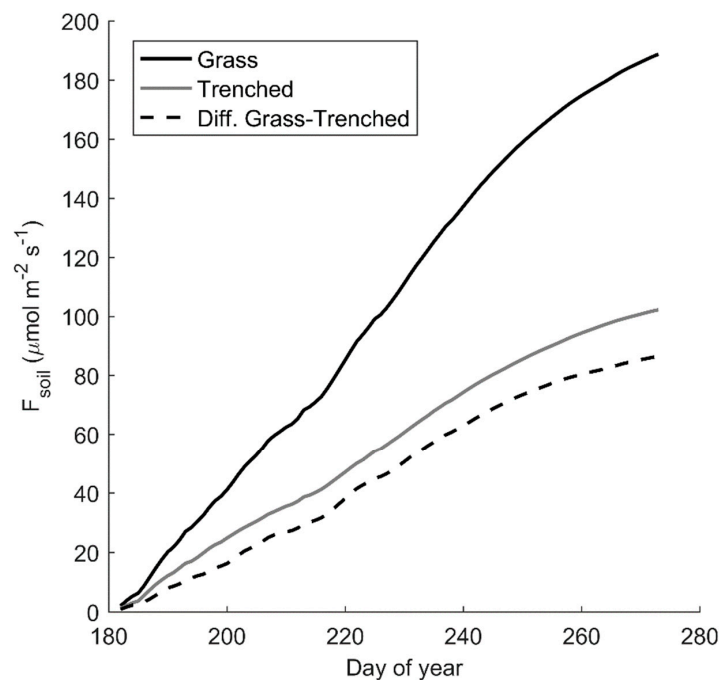


Figure 4. Cumulative daily mean soil CO_2 efflux (F_{soil}) for grass (black) and bare, trenched intercanopy soil (gray) during the 2017 experiment comparison period at the grassland site. The grass-trenched difference (dashed) is an estimate of belowground autotrophic respiration.

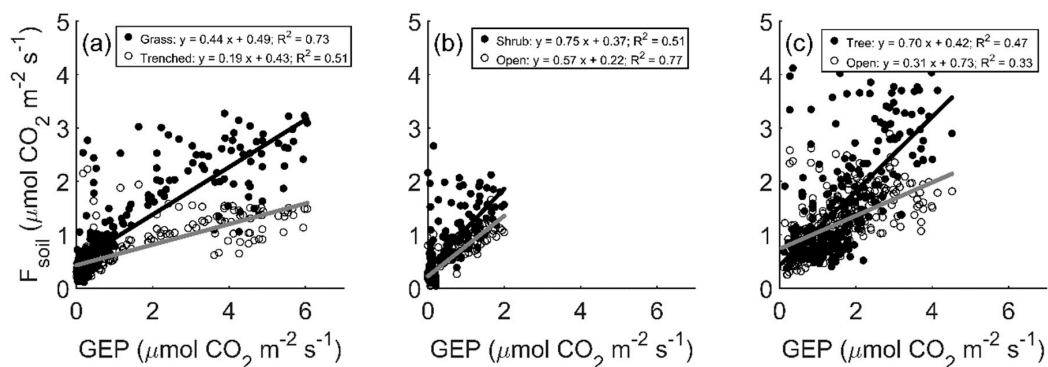


Figure 5. Linear relationship between daily mean soil CO_2 efflux (F_{soil}) and gross ecosystem photosynthesis (GEP) at the grassland (a), shrubland (b), and savanna (c) sites. Closed circles indicate plots near or under vegetation canopies, and open circles are for plots either trenched (a) or between shrub/tree canopies (b,c).

3.4. Model Performance

To integrate these varied environmental controls on F_{soil} we used a multivariate modeling approach by sequentially adding T_s , θ , and GEP as explanatory variables. For the grassland, we tested the ability of data-informed models to predict temporal variability in F_{soil} . The model based solely on T_s (Equation (1)) explained less than 40% of the variation in observed daily mean F_{soil} for the grass and trenched plots (Table 2). As shown in Sections 3.2 and 3.3, the temperature response of F_{soil} varied strongly with θ and the magnitude of F_{soil} was related to GEP . Models that represented these observed effects of θ (Equation (2)) and GEP (Equation (3)) on F_{soil} outperformed Equation (1), as indicated by higher R^2 lower AIC , and lower $RMSE$ (Table 2). For the grass plots, adding either a moisture or photosynthesis term to Equation (1) increased R^2 to a similar degree. Conversely, in the trenched plots that were manipulated to exclude root activity associated with photosynthesis, goodness of fit metrics show that the model with a moisture term (Equation (2)) was better than the model with a photosynthesis term (Equation (3)). The complete model—which included temperature, moisture, and photosynthesis terms (Equation (4))—outperformed less complex models in the grass plots. However, in the trenched plots that were uninfluenced by GEP , Equations (2) and (4) explained a similar amount of variation in F_{soil} but Equation (4) had lower AIC .

We also tested the models at the shrubland and savanna to determine if the trend in performance was consistent across sites with different vegetation. As in the grassland, temperature alone was a poor predictor of variation in F_{soil} , and adding moisture (Equation (2)) or photosynthesis (Equation (3)) terms strongly improved model performance (Table 2). Adding a moisture term to the temperature-based model explained more variation in F_{soil} than did adding a photosynthesis term (Table 2). To test if this difference in relative explanatory power was related to the timing of photosynthesis relative to microbial respiration of root exudates, we used cross-correlation analysis to investigate lags between F_{soil} and GEP . Correlation was maximized when F_{soil} was lagged relative to GEP by zero days in the grassland, one day in the shrubland, and two days in the savanna (Table 3). Applying these lags and re-fitting the models increased the amount of variation in F_{soil} explained by Equation (3) to be comparable to Equation (2) at the shrubland and savanna. The complete model (Equation (4)) performed best in the shrubland and savanna. As indicated by lower AIC , Equation (4) improved model performance most in the savanna—which is also where we observed the weakest coupling between daily mean GEP and θ and the largest F_{soil} – GEP lag among sites (Table 3). We found that the relative explanatory value of model drivers varied among sites (Table 2).

Table 2. Fitted model (Equations (1)–(4)) parameters and the coefficient of determination (R^2), Akaike information criterion (AIC), and root mean squared error (RMSE, $\mu\text{mol CO}_2 \text{ m}^{-2} \text{ s}^{-1}$) used to assess model performance at the grassland, shrubland, and savanna sites. Bold numbers indicate best performance among model groups (highest R^2 ; lowest AIC; lowest RMSE).

Site	Plot	Model	Drivers	F_{ref}	b	c	n	n	R^2	AIC	RMSE
Grassland	Grass	1	T_s	0.44	0.04	-	-	244	0.12	568	0.80
	Grass	2	T_s, θ	0.75	0.04	69.38	-	244	0.75	268	0.42
	Grass	3	T_s, GEP	1.10	0.04	-	0.23	244	0.77	252	0.41
	Grass	4	T_s, θ, GEP	0.99	0.04	56.54	0.84	244	0.86	142	0.33
Grassland	Trenched	1	T_s	0.18	0.06	-	-	154	0.37	169	0.42
	Trenched	2	T_s, θ	0.43	0.04	95.93	-	154	0.79	3	0.24
	Trenched	3	T_s, GEP	0.35	0.06	-	0.53	154	0.65	79	0.31
	Trenched	4	T_s, θ, GEP	0.47	0.04	89.34	3.80	154	0.80	-3	0.24
Shrubland	Shrub	1	T_s	0.76	0.00	-	-	164	0.00	293	0.59
	Shrub	2	T_s, θ	2.61	-0.02	103.63	-	164	0.66	119	0.35
	Shrub	3	T_s, GEP	2.11	0.00	-	0.24	164	0.50	182	0.42
	Shrub	4	T_s, θ, GEP	3.02	-0.02	98.56	2.03	164	0.68	108	0.34
	Shrub *	3 *	$T_s, GEP *$	1.76	0.01	-	0.18	163	0.63	130	0.36
	Shrub *	4 *	$T_s, \theta, GEP *$	3.18	-0.02	96.89	1.25	163	0.74	76	0.31
Savanna	Tree	1	T_s	0.85	0.03	-	-	255	0.05	711	0.98
	Tree	2	T_s, θ	1.42	0.03	55.50	-	255	0.54	526	0.68
	Tree	3	T_s, GEP	2.82	0.01	-	0.18	255	0.41	591	0.77
	Tree	4	T_s, θ, GEP	3.04	0.01	47.92	0.61	255	0.64	466	0.60
	Tree *	3 *	$T_s, GEP *$	3.07	0.01	-	0.11	253	0.52	532	0.69
	Tree *	4 *	$T_s, \theta, GEP *$	3.18	0.01	44.11	0.41	253	0.69	423	0.56

Models 1–4 have the form of Equations (1)–(4) described in Section 2.5. F_{soil} is soil CO_2 efflux; θ is volumetric soil moisture; θ_{opt} is the optimal θ for F_{soil} ; GEP is gross ecosystem photosynthesis; GEP_{max} is the maximum value of GEP . Each row lists the model parameters (F_{ref} , b , c , and n). * indicates models in which F_{soil} was lagged relative to GEP (1 day at shrubland; 2 days at the savanna) based on results from a cross-correlation analysis.

Table 3. Lag times for maximum cross-correlation between daily means of gross ecosystem photosynthesis (GEP) and soil CO_2 efflux (F_{soil}). Also shown is the coefficient of determination (R^2) of linear regressions between un-lagged and lagged daily mean θ and GEP for the grassland, shrubland, and savanna sites.

Site	Lag (Days)	R^2	
		$GEP-F_{soil}$	$GEP-\theta$
Grassland	0	0.53	-
Shrubland	1	0.34	0.47
Savanna	2	0.14	0.26

All regressions significant at $p < 0.01$.

Importantly, model drivers influenced temporal dynamics in predicted F_{soil} (Figures 6 and 7). Equation (1) (T_s) failed to reproduce the seasonality observed in F_{soil} , generally over-predicting F_{soil} during the dry pre-monsoon period and under-predicting F_{soil} during the growing season (Figure 6, Figures S11 and S12). Adding a moisture term to the temperature-based model improved predicted seasonality in F_{soil} because it better captured variability in observed F_{soil} and predicted high F_{soil} immediately following rain events at the monsoon onset. However, Equation (2) tended to underestimate growing season F_{soil} since it did not represent the stimulating effect of GEP on F_{soil} (Figure 4). Adding a photosynthesis term (Equation (3)) better predicted the magnitude of growing season F_{soil} but was delayed relative to observations due to lags between the onset of high θ and GEP upregulation. Thus, the inclusion of both moisture and photosynthesis terms in Equation (4) was required to model the seasonality, magnitude, and variability in F_{soil} at all sites (Figure 7).

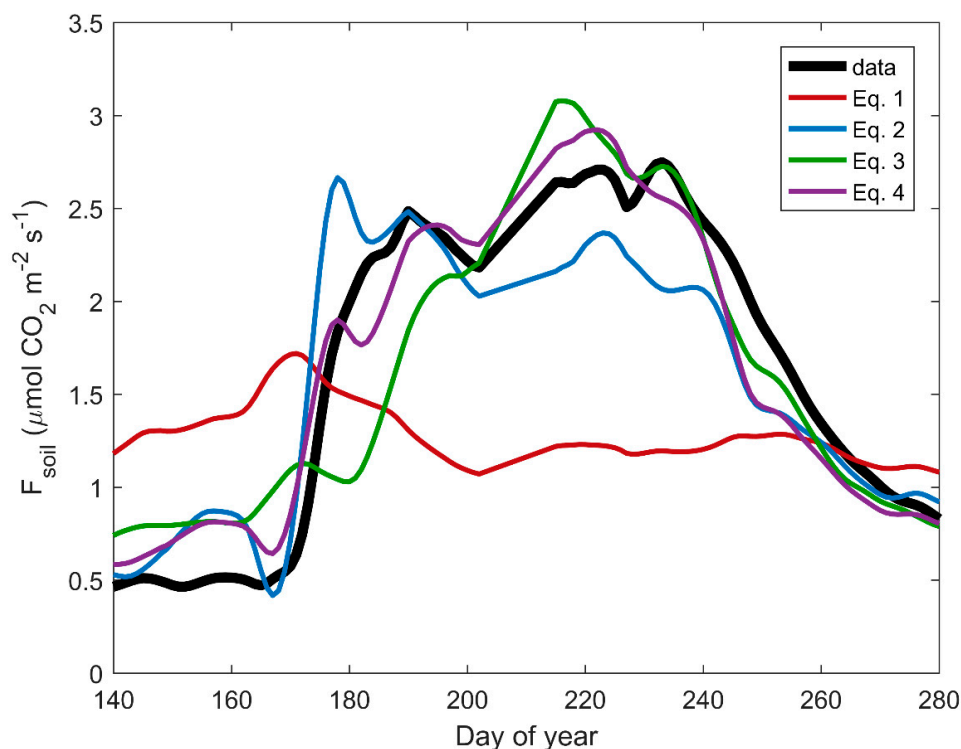


Figure 6. Loess smoothed temporal dynamics in daily mean observed (black) and predicted (color) soil CO_2 efflux (F_{soil}) at the grassland site. Equation (1) is based on an exponential relationship between F_{soil} and soil temperature (T_s), whereas Equations (2) and (3) combine Equation (1) with volumetric soil moisture (θ) and gross ecosystem photosynthesis (GEP) terms, respectively. Equation (4) is the complete model with T_s , θ , and GEP terms.

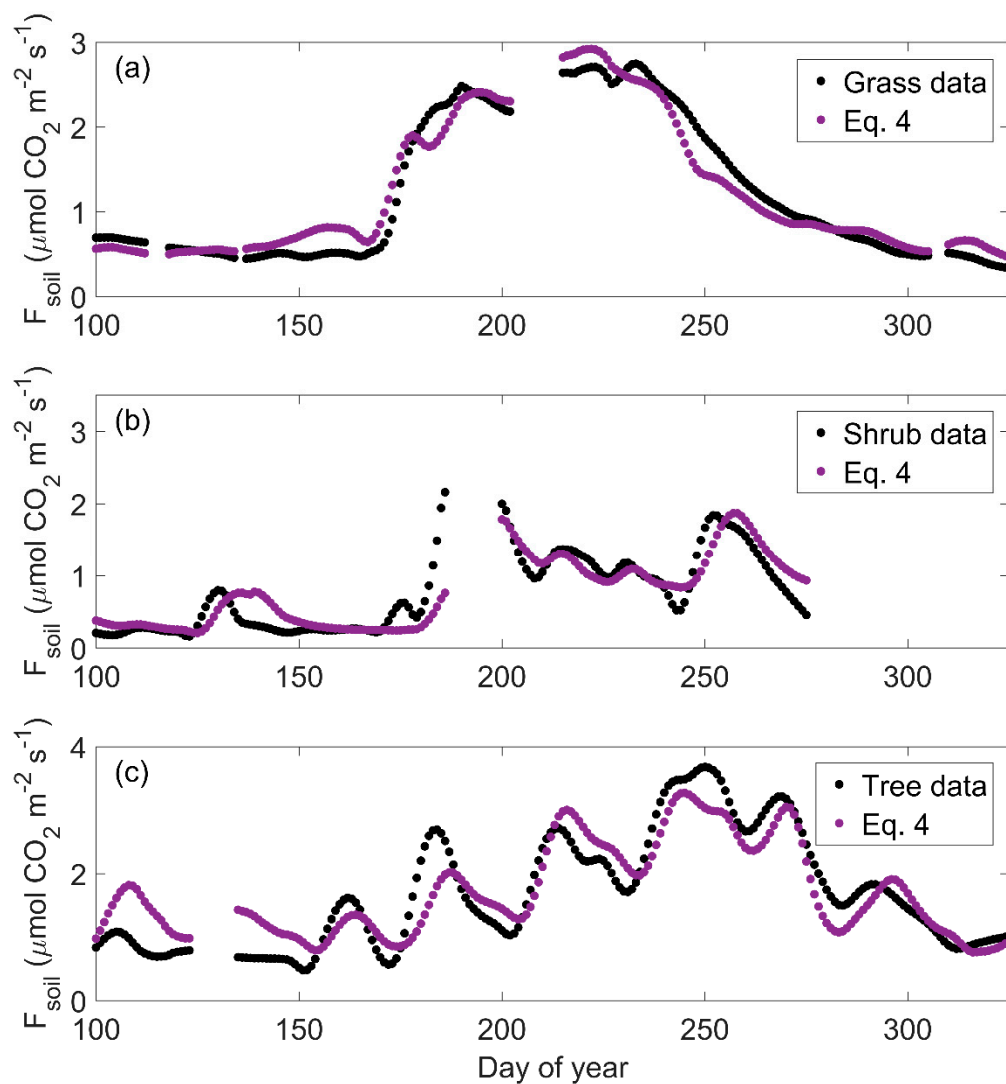


Figure 7. Loess smoothed temporal dynamics in daily mean observed (black) and predicted (purple) soil CO₂ efflux (F_{soil}) at the grassland (a), shrubland (b), and savanna (c) sites. Equation (4) is the complete model with soil temperature (T_s), volumetric soil moisture (θ) and gross ecosystem photosynthesis (GEP) terms.

4. Discussion

In three semiarid ecosystems we found that T_s , θ , and GEP influenced the dynamics, magnitude, and variability of F_{soil} . Water availability strongly influenced F_{soil} rates and patterns, whereas GEP stimulated F_{soil} , particularly for plots near vegetation. These results provide additional evidence that moisture availability regulates temporal variation in F_{soil} , and biological factors impact spatial variation in F_{soil} [10,11,13,52]. The complete model (Equation (4)) integrated T_s , θ , and GEP controls and better captured temporal dynamics in observed F_{soil} than less complex models. Testing the model across sites with similar climate forcing indicated that the explanatory value of model drivers varied with vegetation structure and productivity. Together, these results show that models that account for T_s , θ , and GEP can represent how F_{soil} responds to changes in water availability and vegetation activity in ecosystems with varying structure.

4.1. Water Availability Limits Autotrophic and Heterotrophic Respiration

The temperature response of F_{soil} was conditional on θ (Figure 3). Modeling these interactions is important since warming-driven reductions in θ can suppress F_{soil} despite higher T_s [23]. In the

grassland, high θ enhanced the temperature sensitivity of F_{soil} , whereas low θ suppressed F_{soil} in the grass and trenched plots (Figure 3), which indicates that water availability constrains both R_a and R_h . Low soil moisture can inhibit R_h by decreasing substrate availability, microbial activity, solute transport, or some combination of these drivers [23,29,53,54]. Moisture limitation may also suppress R_a through reductions in root exudates due to decreased rates of photosynthesis and phloem transport in water-stressed plants [23,55]. Thus, changes in moisture availability can cause seasonal variation in the magnitude and temperature response of F_{soil} in semiarid ecosystems, as previously found in mesic forests [38]. Models that account for interactions between T_s and θ are more apt to capture seasonality and pulsed dynamics in F_{soil} that impact the carbon balance of semiarid ecosystems [7,56]. The need to represent water stress effects on F_{soil} is likely to apply beyond semiarid ecosystems since most regions already experience periods of water limitation [57] and drylands are projected to expand [19].

4.2. Ecosystem Photosynthesis Stimulates Soil CO₂ Efflux

The link between GEP and F_{soil} contributes to spatial variation in F_{soil} rates (Figure 5). We found that recent photosynthesis impacts F_{soil} likely through enhanced root respiration and the stimulating effect of root exudation on microbial respiration (Figure 5, Tables 2 and 3), which has been reported across a variety of ecosystems [11,35,37,39,58]. Even when θ was similar, growing season rates of F_{soil} were greater for plots near vegetation (Figures 2 and 3). Even though the shrubland and savanna did not have trenched plots, F_{soil} closer to the vegetation was higher and responded more strongly to photosynthesis variation. Despite the uncertainty in GEP due to NEE measurement and partitioning bias, and differences in measurement scale, GEP was correlated with F_{soil} and was important to predict temporal dynamics in F_{soil} (Table 3; [13]). Note that since GEP used here is an ecosystem-scale flux, and photosynthetic inputs are likely to vary across space (Figures 3 and 4), predictive models of F_{soil} could be improved if new tools to disaggregate ecosystem flux measurements were used to determine the spatial distribution of GEP [59].

The effects of GEP on F_{soil} are illustrated by seasonal changes in F_{soil} partitioning. We found that the difference in F_{soil} between plots increased as the growing season progressed (Figure 2, Figures S1 and S2), and F_{soil} was greater and more sensitive to GEP for plots near vegetation (Figure 5), as previously reported in this region [13]. These dynamics are likely linked to plant physiology and phenology, which have been shown to affect the magnitude and partitioning of F_{soil} in temperate forests [41,60] and California grasslands [11]. Applying the model at the grassland showed that GEP had a stronger effect on F_{soil} for the grass plots (Table 2; low n : strong GEP effect on F_{soil}) than the trenched plots (high n : weak GEP effect on F_{soil}). At the grassland, our estimate of R_a (difference in F_{soil} between the grass and trenched plots) correlated strongly with GEP ($R^2 = 0.66$) and was a considerable fraction (44%) of total growing season F_{soil} (Figure 4). While we did not have trenched plots at the shrubland and savanna to partition F_{soil} , differences in the seasonal pattern of F_{soil} for plots that differed in their proximity to vegetation indicate that R_a is likely also a considerable fraction of F_{soil} at these sites (Figure 5, Figures S1 and S2). Our estimate of the growing season $R_a:F_{soil}$ ratio for the grassland is lower than the mean value reported in a review of grass and crop ecosystems (60.4%; [61]) but similar to results from a mesic grassland (48–52%; [62]). Since R_a can be a significant component of F_{soil} in ecosystems that span a wide range of water availability, refined understanding of controls on R_a is necessary to reduce uncertainty in F_{soil} .

4.3. Moisture and Photosynthesis Terms Improve Modeled Carbon-Water Dynamics

Model predictions based solely on temperature do not accurately reflect F_{soil} in water-limited ecosystems. However, by explicitly representing the combined effects of T_s , θ , and GEP , the full model (Equation (4)) predicted temporal variation in observed F_{soil} associated with dynamics in moisture availability and vegetation activity across structurally diverse sites (Figure 7). At the shrubland in particular, Equation (4) explained 74% of the variation in daily mean F_{soil} even though we did not

observe a relationship between F_{soil} and T_s (Table 2). Decoupling between F_{soil} and T_s when moisture was limiting (Figure 3) likely explains why the temperature-only model (Equation (1)) did not capture seasonal dynamics in F_{soil} (Figure 6). By adding θ to a temperature-based model, predicted F_{soil} was suppressed when water was limiting and enhanced when θ was optimal (Figure 6). Together, T_s and θ explained more than 50% of the observed variability across sites (Table 2). The superior performance of Equation (2) over Equations (1) and (3) across sites with different vegetation structure underscores that water availability is a key control on respiration processes in semiarid ecosystems (Table 2).

While supplementing a temperature-based model with either θ or GEP terms increased the amount of explained variation in F_{soil} to a similar degree, the combination of T_s , θ , and GEP was required to maximize model performance and predict seasonality in F_{soil} . Models that accounted for θ captured the pulsed increase in metabolic activity at the monsoon onset characteristic of semiarid ecosystems [12,21,63], whereas GEP terms improved the prediction of F_{soil} magnitude and seasonality by reflecting the stimulating effect of photosynthesis on basal F_{soil} ([39]; Figure 6). We found that F_{soil} increased rapidly in response to increased θ at the beginning of the monsoon, whereas GEP increased more gradually (Figure 2), which reflect differences in the timing of ecosystem responses to rainfall pulses [56]. While these results indicate that this model captures F_{soil} dynamics in these subtropical, warm-season ecosystems, future studies should test this model in cool-season desert ecosystems. We also found that predictions from GEP -based models lagged observed F_{soil} . Previous research has documented lags between GEP and F_{soil} ranging from hourly to daily timescales depending on the vegetative cover and time of year [22,31,37,64]. Consistent with previous research, no lag was detected at the grassland [65]. However, applying one or two days of lag between GEP and F_{soil} improved model performance at the shrubland and savanna (Table 2). These results provide additional evidence in support of incorporating lag information in semi-empirical F_{soil} models [65]. Together, our findings indicate that models with T_s , θ , and GEP terms can better capture rainfall-driven pulses in carbon dynamics than simpler models [56].

4.4. Vegetation Activity and Structure Influence the Relative Importance of Soil CO_2 Efflux Drivers

The degree of vegetation activity influences the relative importance of F_{soil} controls. In the grassland, F_{soil} for grass plots was more sensitive to GEP (Table 2; low n), whereas F_{soil} for trenched plots was more sensitive to θ (high c). This result is consistent with our expectation that θ would more strongly regulate F_{soil} from plots manipulated to exclude the effects of GEP on belowground activity. Similarly, F_{soil} was more sensitive to θ than GEP (Table 2; high c , high n) at sites with low cumulative GEP (shrubland, grassland trenched plots). We observed unexpected differences between sites in how θ influenced the relationship between F_{soil} and T_s . Contrary to the grassland, the effect of θ on the relationship between F_{soil} and T_s was weaker in the savanna and was not observed in the shrubland (Figure 3, Figures S9 and S10). Previous work in this region found that the temperature sensitivity of F_{soil} was lower during wet conditions in grass plots but not influenced by moisture in plots near mesquite trees [37]. The complete model captured how vegetation modulated the effects of environmental controls on F_{soil} and therefore may be applicable in various ecosystems subject to water limitation.

Interactions between vegetation structure and carbon-water coupling can help explain site differences in the explanatory power of F_{soil} controls. Vegetation can cause decoupling and lags between F_{soil} and its controls [16,34] due to plant structure and rooting characteristics. Previous work in this region found that F_{soil} was more sensitive to antecedent photosynthesis rates in mesquite plots, whereas F_{soil} near grass plots was more influenced by same-day photosynthesis [37]. Similarly, we found greater lag between GEP and F_{soil} (Table 3) at the savanna (two days) and shrubland (one day) than the grassland (zero days), perhaps due to larger structure and longer phloem transport distance for the woody plants [22,37]. While θ and GEP controls were interchangeable for the grass plots, θ had greater explanatory power than unlagged GEP in the shrubland and savanna. Lagging GEP made its explanatory power comparable to θ (Table 2). Thus, we suggest that future semi-empirical

models include terms that account for lag. Differences in lags may be related to variation in rooting characteristics between sites. In the short-rooted grassland, strong coupling between shallow θ and GEP leads to covariation which makes either term suitable to explain variation in F_{soil} . Conversely, trees and shrubs generally have a higher proportion of roots in deep soil than grasses [44], and GEP is more coupled to deeper θ [4,64], leading to more of a disconnect between GEP and shallow θ and their effects on F_{soil} [32,56,66].

F_{soil} drivers suggest that ecosystem composition likely alters the magnitude and spatial variability of F_{soil} . Woody encroachment has been shown to increase F_{soil} variation in semiarid grassland [13] and savanna ecosystems [34]. Vegetation structure and functioning contributes to spatial variation in F_{soil} (Figure 5) and modifies the response of F_{soil} to environmental controls (Figure 3 and Table 2). The strong performance of the complete model across ecosystems with a differing structure indicates that simple models with environmental and vegetative controls [31] may be useful to investigate how changes in ecosystem composition will impact F_{soil} . To increase the utility of this model, further research should focus on how to represent differences in θ - GEP coupling between woody ecosystems and grasslands [67].

5. Conclusions

Temperature, moisture, and photosynthesis were each important controls on F_{soil} in grassland, shrubland, and savanna ecosystems. While models relying on T_s erroneously predicted high F_{soil} before the growing season, those with θ and GEP controls captured variation in F_{soil} associated with dynamics in moisture availability and vegetation activity. This study is novel in that it is the first to test if a F_{soil} model driven by daily T_s , θ , and GEP can capture temporal dynamics and variability in F_{soil} across semiarid sites with similar climate forcing but differing vegetation structure. While the mechanism governing the relative importance of T_s , θ , and GEP controls across sites remains unclear, it is likely related to vegetation characteristics associated with productivity and water use. Our results indicate that this simple model structure can capture F_{soil} dynamics associated with transitions from process-rate limitation to substrate constraints [22]. This study builds upon recent modeling advances [31] and indicates that this type of modeling approach can capture spatial and temporal variation in F_{soil} across structurally diverse, semiarid ecosystems, particularly if time series data of plant function is available. Combining this modeling approach with increased monitoring of F_{soil} at flux tower sites could help investigate connections between plot and ecosystem-scale carbon exchange [47]. Future studies should test this model in cool-season ecosystems, which tend to be temperature-limited when soil moisture is non-limiting [24]. It is reasonable to infer that the relative importance of model drivers would differ between cool-season ecosystems and the warm-season ecosystems examined herein. Accounting for the interactive effects of T_s , θ , and GEP on F_{soil} will be important to determine the response of water-limited ecosystems to changes in climate and land cover.

Supplementary Materials: The following are available online: <http://www.mdpi.com/2571-8789/3/1/6/s1>. Figure S1: Time series of carbon fluxes and controls at the shrubland, Figure S2: Time series of carbon fluxes and controls at the savanna, Figure S3: Relationship between soil moisture and soil CO₂ efflux at the grassland, Figure S4: Relationship between soil moisture and soil CO₂ efflux at the shrubland, Figure S5: Relationship between soil moisture and soil CO₂ efflux at the savanna, Figure S6: Controls on soil CO₂ efflux at the grassland, Figure S7: Controls on soil CO₂ efflux at the shrubland, Figure S8: Controls on soil CO₂ efflux at the savanna, Figure S9: Temperature response of soil CO₂ efflux at the savanna, Figure S10: Temperature response of soil CO₂ efflux at the shrubland, Figure S11: Predicted temporal dynamics of soil CO₂ efflux at the shrubland, Figure S12: Predicted temporal dynamics of soil CO₂ efflux at the savanna.

Author Contributions: R.L.S. designed the experiment with assistance from G.A.B.-G., E.P.H., M.C.R. and D.J.P.M.; M.C.R. and R.L.S. performed the experiment; M.C.R., R.L.S. and D.J.P.M. analyzed the data. M.C.R. wrote the manuscript with input from all coauthors.

Funding: This work was supported by USDA-ARS and funding for these AmeriFlux Core Sites (US-SRM, US-Wkg, and US-Whs) was also provided by the U.S. Department of Energy Berkeley National Labs.

Acknowledgments: The soil CO₂ efflux data used in this study are available upon request to the corresponding author. Eddy covariance flux data used in this paper are available at the AmeriFlux Data Repository

(<http://ameriflux.lbl.gov/>) or upon request to the corresponding author. Phenocam imagery is available at <http://https://phenocam.sr.unh.edu>. This work was supported by USDA-ARS and funding for these AmeriFlux Core Sites (US-SRM, US-Wkg, and US-Whs) was also provided by the U.S. Department of Energy Berkeley National Labs. We thank R. Bryant for his expert technical assistance in maintaining the instrumentation at the sites. M.C.R. thanks R. Canales for assistance with data analysis. USDA-ARS is an equal opportunity employer.

Conflicts of Interest: The authors declare no conflict of interest.

References

1. Poulter, B.; Frank, D.; Ciais, P.; Myneni, R.B.; Andela, N.; Bi, J.; Broquet, G.; Canadell, J.G.; Chevallier, F.; Liu, Y.Y.; Running, S.W.; et al. Contribution of semi-arid ecosystems to interannual variability of the global carbon cycle. *Nature* **2014**, *509*, 600–603. [[CrossRef](#)] [[PubMed](#)]
2. Ahlström, A. The dominant role of semiarid ecosystems in the trend and variability of the land CO₂ sink. *Science* **2015**, *348*, 895–899. [[CrossRef](#)] [[PubMed](#)]
3. Valentini, R.; Matteucci, G.; Dolman, A.J.; Schulze, E.; Rebmann, C.; Moors, E.J.; Granier, A.; Gross, P.; Jensen, N.O. Respiration as the main determinant of carbon balance in European forests. *Nature* **2000**, *404*, 861–865. [[CrossRef](#)] [[PubMed](#)]
4. Scott, R.L.; Hamerlynck, E.P.; Jenerette, G.D.; Moran, M.S.; Gafford, G.A.B. Carbon dioxide exchange in a semidesert grassland through drought-induced vegetation change. *J. Geophys. Res.* **2010**, *115*, 1–12. [[CrossRef](#)]
5. Hamerlynck, E.P.; Scott, R.L.; Sánchez-Cañete, E.P.; Barron-Gafford, G.A. Nocturnal soil CO₂ uptake and its relationship to subsurface soil and ecosystem carbon fluxes in a Chihuahuan Desert shrubland. *J. Geophys. Res. Biogeosci.* **2013**, *118*, 1593–1603. [[CrossRef](#)]
6. Ryan, M.G.; Law, B.E. Interpreting, measuring, and modeling soil respiration. *Biogeochemistry* **2005**, *73*, 3–27. [[CrossRef](#)]
7. Sánchez-Cañete, E.P.; Scott, R.L.; van Haren, J.; Barron-Gafford, G.A. Improving the accuracy of the gradient method for determining soil carbon dioxide efflux: Accurate Long-Term F_{soil} Based on the GM. *J. Geophys. Res. Biogeosci.* **2017**, *122*, 50–64. [[CrossRef](#)]
8. Lloyd, J.; Taylor, J.A. On the temperature dependence of soil respiration. *Source Funct. Ecol.* **1994**, *8*, 315–323. [[CrossRef](#)]
9. Davidson, E.A.; Belk, E.; Boone, R.D. Soil water content and temperature as independent of confounded factors controlling soil respiration in a temperate mixed hardwood forest. *Glob. Chang. Biol.* **1998**, *4*, 217–227. [[CrossRef](#)]
10. Xu, M.; Qi, Y. Soil surface CO₂ efflux and its spatial and temporal variations in a young ponderosa pine plantation in northern California. *Glob. Chang. Biol.* **2001**, *7*, 667–677. [[CrossRef](#)]
11. Tang, J.; Baldocchi, D.D. Spatial-temporal variation in soil respiration in an oak-grass savanna ecosystem in California and its partitioning into autotrophic and heterotrophic components. *Biogeochemistry* **2005**, *73*, 183–207. [[CrossRef](#)]
12. Sponseller, R.A. Precipitation pulses and soil CO₂ flux in a Sonoran Desert ecosystem. *Glob. Chang. Biol.* **2007**, *13*, 426–436. [[CrossRef](#)]
13. Cable, J.M.; Barron-Gafford, G.A.; Ogle, K.; Pavao-Zuckerman, M.; Scott, R.L.; Williams, D.G.; Huxman, T.E. Shrub encroachment alters sensitivity of soil respiration to temperature and moisture. *J. Geophys. Res. Biogeosci.* **2012**, *117*. [[CrossRef](#)]
14. Reichstein, M.; Rey, A.; Freibauer, A.; Tenhunen, J.; Valentini, R.; Banza, J.; Casals, P.; Cheng, Y.; Grünzweig, J.M.; Irvine, J.; et al. Modeling temporal and large-scale spatial variability of soil respiration from soil water availability, temperature and vegetation productivity indices. *Glob. Biogeochem. Cycles* **2003**, *17*. [[CrossRef](#)]
15. Wang, B.; Zha, T.S.; Jia, X.; Gong, J.N.; Bourque, C.; Feng, W.; Tian, Y.; Wu, B.; Qing Zhang, Y.; Peltola, H. Soil water regulates the control of photosynthesis on diel hysteresis between soil respiration and temperature in a desert shrubland. *Biogeosciences* **2017**, *14*, 3899–3908. [[CrossRef](#)]
16. Vargas, R.; Allen, M.F. Environmental controls and the influence of vegetation type, fine roots and rhizomorphs on diel and seasonal variation in soil respiration. *New Phytol.* **2008**, *179*, 460–471. [[CrossRef](#)]
17. Xu, M.; Shang, H. Contribution of soil respiration to the global carbon equation. *J. Plant Physiol.* **2016**, *203*, 16–28. [[CrossRef](#)]

18. Xu, L.; Baldocchi, D.D.; Tang, J. How soil moisture, rain pulses, and growth alter the response of ecosystem respiration to temperature. *Glob. Biogeochem. Cycles* **2004**, *18*. [[CrossRef](#)]
19. Feng, S.; Fu, Q. Expansion of global drylands under a warming climate. *Atmos. Chem. Phys.* **2013**, *13*, 10081–10094. [[CrossRef](#)]
20. Huang, J.; Yu, H.; Guan, X.; Wang, G.; Guo, R. Accelerated dryland expansion under climate change. *Nat. Clim. Chang.* **2016**, *6*, 166. [[CrossRef](#)]
21. Jenerette, G.D.; Scott, R.L.; Huxman, T.E. Whole ecosystem metabolic pulses following precipitation events. *Funct. Ecol.* **2008**, *22*, 924–930. [[CrossRef](#)]
22. Kuzyakov, Y.; Gavrichkova, O. Time lag between photosynthesis and carbon dioxide efflux from soil: A review of mechanisms and controls. *Glob. Chang. Biol.* **2010**, *16*, 3386–3406. [[CrossRef](#)]
23. Liu, W.; Zhang, Z.; Wan, S. Predominant role of water in regulating soil and microbial respiration and their responses to climate change in a semiarid grassland. *Glob. Chang. Biol.* **2009**, *15*, 184–195. [[CrossRef](#)]
24. Cable, J.M.; Ogle, K.; Lucas, R.W.; Huxman, T.E.; Loik, M.E.; Smith, S.D.; Tissue, D.T.; Ewers, B.E.; Pendall, E.; Welker, J.M.; et al. The temperature responses of soil respiration in deserts: A seven desert synthesis. *Biogeochemistry* **2011**, *103*, 71–90. [[CrossRef](#)]
25. Bond-Lamberty, B.; Thomson, A. A global database of soil respiration data. *Biogeosciences* **2010**, *7*, 1915–1926. [[CrossRef](#)]
26. Yan, Z.; Bond-Lamberty, B.; Todd-Brown, K.E.; Bailey, V.L.; Li, S.; Liu, C.; Liu, C. A moisture function of soil heterotrophic respiration that incorporates microscale processes. *Nat. Commun.* **2018**, *9*, 2562. [[CrossRef](#)] [[PubMed](#)]
27. Tang, J.; Baldocchi, D.D.; Xu, L. Tree photosynthesis modulates soil respiration on a diurnal time scale. *Glob. Chang. Biol.* **2005**, *11*, 1298–1304. [[CrossRef](#)]
28. Conant, R.T.; Klopatek, J.M.; Klopatek, C.C. Environmental factors controlling soil respiration in three semiarid ecosystems. *Soil Sci. Soc. Am. J.* **2000**, *64*, 383–390. [[CrossRef](#)]
29. Jassal, R.S.; Black, T.A.; Novak, M.D.; Gaumont-Guay, D.; Nesic, Z. Effect of soil water stress on soil respiration and its temperature sensitivity in an 18-year-old temperate Douglas-fir stand. *Glob. Chang. Biol.* **2008**, *14*, 1305–1318. [[CrossRef](#)]
30. Luo, Y.; Ahlström, A.; Allison, S.D.; Batjes, N.H.; Brovkin, V.; Carvalhais, N.; Chappell, A.; Ciais, P.; Davidson, E.A.; Finzi, A.; et al. Toward more realistic projections of soil carbon dynamics by Earth system models. *Glob. Biogeochem. Cycles* **2016**, *30*, 40–56. [[CrossRef](#)]
31. Zhang, Q.; Phillips, R.P.; Manzoni, S.; Scott, R.L.; Oishi, A.C.; Finzi, A.; Daly, E.; Vargas, R.; Novick, K.A. Changes in photosynthesis and soil moisture drive the seasonal soil respiration-temperature hysteresis relationship. *Agric. For. Meteorol.* **2018**, *259*, 184–195. [[CrossRef](#)]
32. Jackson, R.B.; Canadell, J.; Ehleringer, J.R.; Mooney, H.A.; Sala, O.E.; Schulze, E.D. A global analysis of root distributions for terrestrial biomes. *Oecologia* **1996**, *108*, 389–411. [[CrossRef](#)] [[PubMed](#)]
33. Nadezhdina, N.; David, T.S.; David, J.S.; Ferreira, M.I.; Dohnal, M.; Tesař, M.; Gartner, K.; Leitgeb, E.; Nadezhdin, V.; Cermak, J.; et al. Trees never rest: The multiple facets of hydraulic redistribution. *Ecohydrology* **2010**, *3*, 431–444. [[CrossRef](#)]
34. Barron-Gafford, G.A.; Scott, R.L.; Jenerette, G.D.; Huxman, T.E. The relative controls of temperature, soil moisture, and plant functional group on soil CO₂ efflux at diel, seasonal, and annual scales. *J. Geophys. Res. Biogeosci.* **2011**, *116*. [[CrossRef](#)]
35. Curiel Yuste, J.; Baldocchi, D.D.; Gershenson, A.; Goldstein, A.; Misson, L.; Wong, S. Microbial soil respiration and its dependency on carbon inputs, soil temperature and moisture. *Glob. Chang. Biol.* **2007**, *13*, 2018–2035. [[CrossRef](#)]
36. Cable, J.M.; Ogle, K.; Williams, D.G.; Weltzin, J.F.; Huxman, T.E. Soil texture drives responses of soil respiration to precipitation pulses in the sonoran desert: Implications for climate change. *Ecosystems* **2008**, *11*, 961–979. [[CrossRef](#)]
37. Barron-Gafford, G.A.; Cable, J.M.; Bentley, L.P.; Scott, R.L.; Huxman, T.E.; Jenerette, G.D.; Ogle, K. Quantifying the timescales over which exogenous and endogenous conditions affect soil respiration. *New Phytol.* **2014**, *202*, 442–454. [[CrossRef](#)]
38. Suseela, V.; Conant, R.T.; Wallenstein, M.D.; Dukes, J.S. Effects of soil moisture on the temperature sensitivity of heterotrophic respiration vary seasonally in an old-field climate change experiment. *Glob. Chang. Biol.* **2012**, *18*, 336–348. [[CrossRef](#)]

39. Sampson, D.A.; Janssens, I.A.; Curiel Yuste, J.; Ceulemans, R. Basal rates of soil respiration are correlated with photosynthesis in a mixed temperate forest. *Glob. Chang. Biol.* **2007**, *13*, 2008–2017. [[CrossRef](#)]
40. Scott-Denton, L. Spatial and temporal controls of soil respiration rate in a high-elevation, subalpine forest. *Soil Biol. Biochem.* **2003**, *35*, 525–534. [[CrossRef](#)]
41. Moore, D.J.P.; Trahan, N.A.; Wilkes, P.; Quaife, T.; Stephens, B.B.; Elder, K.; Desai, A.R.; Negron, J.; Monson, R.K. Persistent reduced ecosystem respiration after insect disturbance in high elevation forests. *Ecol. Lett.* **2013**, *16*, 731–737. [[CrossRef](#)] [[PubMed](#)]
42. Trahan, N.A.; Dynes, E.L.; Pugh, E.; Moore, D.J.P.; Monson, R.K. Changes in soil biogeochemistry following disturbance by girdling and mountain pine beetles in subalpine forests. *Oecologia* **2015**, *177*, 981–995. [[CrossRef](#)] [[PubMed](#)]
43. Scott, R.L.; Biederman, J.A.; Hamerlynck, E.P.; Barron-gafford, G.A. The carbon balance pivot point of southwestern U.S. semiarid ecosystems: Insights from the 21st century drought. *J. Geophys. Res. Biogeosci.* **2015**, *120*, 2612–2624. [[CrossRef](#)]
44. Cox, J.R.; Frasier, G.W.; Renard, K.G. Biomass distribution at grassland and shrubland sites. *Rangelands* **1986**, *8*, 67–68.
45. Scott, R.L.; Jenerette, G.D.; Potts, D.L.; Huxman, T.E. Effects of seasonal drought on net carbon dioxide exchange from a woody-plant-encroached semiarid grassland. *J. Geophys. Res. Biogeosci.* **2009**, *114*. [[CrossRef](#)]
46. Reichstein, M.; Falge, E.; Baldocchi, D.; Papale, D.; Aubinet, M.; Berbigier, P.; Bernhofer, C.; Buchmann, N.; Gilmanov, T.; Granier, A.; et al. On the separation of net ecosystem exchange into assimilation and ecosystem respiration: Review and improved algorithm. *Glob. Chang. Biol.* **2005**, *11*, 1424–1439. [[CrossRef](#)]
47. Barba, J.; Cueva, A.; Bahn, M.; Barron-Gafford, G.A.; Bond-Lamberty, B.; Hanson, P.J.; Jaimes, A.; Kulmala, L.; Pumpanen, J.; Scott, R.L.; et al. Comparing ecosystem and soil respiration: Review and key challenges of tower-based and soil measurements. *Agric. For. Meteorol.* **2018**, *249*, 434–443. [[CrossRef](#)]
48. Andrade, J.M.; Estévez-Pérez, M.G. Statistical comparison of the slopes of two regression lines: A tutorial. *Anal. Chim. Acta* **2014**, *838*, 1–12. [[CrossRef](#)]
49. Savage, K.; Davidson, E.A.; Richardson, A.D.; Hollinger, D.Y. Three scales of temporal resolution from automated soil respiration measurements. *Agric. For. Meteorol.* **2009**, *149*, 2012–2021. [[CrossRef](#)]
50. Yan, L.; Chen, S.; Huang, J.; Lin, G. Differential responses of auto- and heterotrophic soil respiration to water and nitrogen addition in a semiarid temperate steppe. *Glob. Chang. Biol.* **2010**, *16*, 2345–2357. [[CrossRef](#)]
51. Akaike, H. Information theory and an extension of the maximum likelihood principle. In *Selected Papers of Hirotugu Akaike*; Springer: New York, NY, USA, 1998; pp. 199–213.
52. Zeng, X.; Song, Y.; Zhang, W.; He, S. Spatio-temporal variation of soil respiration and its driving factors in semi-arid regions of North China. *Chin. Geogr. Sci.* **2018**, *28*, 12–24. [[CrossRef](#)]
53. Davidson, E.A.; Richardson, A.D.; Savage, K.E.; Hollinger, D.Y. A distinct seasonal pattern of the ratio of soil respiration to total ecosystem respiration in a spruce-dominated forest. *Glob. Chang. Biol.* **2006**, *12*, 230–239. [[CrossRef](#)]
54. Moyano, F.E.; Manzoni, S.; Chenu, C. Responses of soil heterotrophic respiration to moisture availability: An exploration of processes and models. *Soil Biol. Biochem.* **2013**, *59*, 72–85. [[CrossRef](#)]
55. Wang, B.; Zha, T.S.; Jia, X.; Wu, B.; Zhang, Y.Q.; Qin, S.G. Soil moisture modifies the response of soil respiration to temperature in a desert shrub ecosystem. *Biogeosciences* **2014**, *11*, 259–268. [[CrossRef](#)]
56. Huxman, T.E.; Snyder, K.A.; Tissue, D.; Leffler, A.J.; Ogle, K.; Pockman, W.T.; Sandquist, D.R.; Potts, D.L. Precipitation pulses and carbon fluxes in semiarid and arid ecosystems. *Oecologia* **2004**, *141*, 254–268. [[CrossRef](#)] [[PubMed](#)]
57. Jenerette, G.D.; Barron-Gafford, G.A.; Guswa, A.J.; McDonnell, J.J.; Villegas, J.C. Organization of complexity in water limited ecohydrology. *Ecohydrology* **2012**, *5*, 184–199. [[CrossRef](#)]
58. Höglberg, P.; Nordgren, A.; Buchmann, N.; Taylor, A.F.S.; Ekblad, A.; Höglberg, M.N.; Nyberg, G.; Ottosson-Löfvenius, M.; Read, D.J. Large-scale forest girdling shows that current photosynthesis drives soil respiration. *Nature* **2001**, *411*, 789–792. [[CrossRef](#)]
59. Xu, K.; Metzger, S.; Desai, A.R. Upscaling tower-observed turbulent exchange at fine spatio-temporal resolution using environmental response functions. *Agric. For. Meteorol.* **2017**, *232*, 10–22. [[CrossRef](#)]
60. Savage, K.; Davidson, E.A.; Tang, J. Diel patterns of autotrophic and heterotrophic respiration among phenological stages. *Glob. Chang. Biol.* **2013**, *19*, 1151–1159. [[CrossRef](#)]

61. Hanson, P.J.; Edwards, N.T.; Garren, C.T.; Andrews, J.A. Separating root and soil microbial contributions to soil respiration: A review of methods and observations. *Biogeochemistry* **2000**, *48*, 115–146. [[CrossRef](#)]
62. Gomez-Casanovas, N.; Matamala, R.; Cook, D.R.; Gonzalez-Meler, M.A. Net ecosystem exchange modifies the relationship between the autotrophic and heterotrophic components of soil respiration with abiotic factors in prairie grasslands. *Glob. Chang. Biol.* **2012**, *18*, 2532–2545. [[CrossRef](#)]
63. Vargas, R.; Sánchez-Cañete, P.E.; Serrano-Ortiz, P.; Curiel Yuste, J.; Domingo, F.; López-Ballesteros, A.; Oyonarte, C. Hot-moments of soil CO₂ efflux in a water-limited grassland. *Soil Syst.* **2018**, *2*, 47. [[CrossRef](#)]
64. Baldocchi, D.; Tang, J.; Xu, L. How switches and lags in biophysical regulators affect spatial-temporal variation of soil respiration in an oak-grass savanna. *J. Geophys. Res. Biogeosci.* **2006**, *111*. [[CrossRef](#)]
65. Vargas, R.; Baldocchi, D.D.; Allen, M.F.; Bahn, M.; Black, T.A.; Collins, S.L.; Yuste, J.C.; Hirano, T.; Jassal, R.S.; Pumpanen, J.; et al. Looking deeper into the soil: Biophysical controls and seasonal lags of soil CO₂ production and efflux. *Ecol. Appl.* **2010**, *20*, 1569–1582. [[CrossRef](#)] [[PubMed](#)]
66. Kurc, S.A.; Small, E.E. Soil moisture variations and ecosystem-scale fluxes of water and carbon in semiarid grassland and shrubland. *Water Resour. Res.* **2007**, *43*. [[CrossRef](#)]
67. Jenerette, G.D.; Scott, R.L.; Barron-Gafford, G.A.; Huxman, T.E. Gross primary production variability associated with meteorology, physiology, leaf area, and water supply in contrasting woodland and grassland semiarid riparian ecosystems. *J. Geophys. Res. Biogeosci.* **2009**, *114*. [[CrossRef](#)]



© 2019 by the authors. Licensee MDPI, Basel, Switzerland. This article is an open access article distributed under the terms and conditions of the Creative Commons Attribution (CC BY) license (<http://creativecommons.org/licenses/by/4.0/>).